$Ba_2La_2Cu_2Sn_2O_{11}$: A New Layered Perovskite with a Modulated Structure

Mark T. Anderson and Kenneth R. Poeppelmeier*

Department of Chemistry and the Science and Technology Center for Superconductivity, Northwestern University, Evanston, Illinois 60208

Jin-Ping Zhang, Han-Jie Fan, and Laurence D. Marks*

Department of Materials Science and the Science and Technology Center for Superconductivity, Northwestern University, Evanston, Illinois 60208

Received June 10, 1992. Revised Manuscript Received August 21, 1992

The average structure of the oxygen-deficient perovskite $Ba_2La_2Cu_2Sn_2O_{11}$ can be described by a tetragonal $1a_p \times 1a_p \times 4a_p$ subcell that has $P4/mmm$ space group symmetry and cell parameters $a = 3.9893$ (3), $c = 16.232$ (1) Å. The subcell does not fully describe the long-range structural features. The structure is periodic only in a statistical sense and contains long-period commensurate modulations that have a dominant periodicity (superlattice) or $\sqrt{2}a_p \times \sqrt{2}a_p \times 24a_p$. The structure was determined from a combination of powder X-ray diffraction, time-of-flight neutron diffraction, and transmission electron microscopy. The structure contains copper–oxygen double layers that are interleaved by tin–oxygen double layers. The oxygen vacancies order between copper–oxygen layers and result in the now-familiar square pyramidal coordination of copper. The tin–oxygen octahedra are rotated around [001], and the short-range order ($24a_p$, ≈100 Å) of the sense of the rotations is believed to give rise to the structural modulation. The magnetic susceptibility versus temperature profile indicates the compound is paramagnetic to 4 K.

Introduction

Layered copper oxides that contain small metal ions (B cations) in addition to copper[1-8] provide advantages over simple cuprates in the exploration of the solid-state chemistry that underlies high-temperature superconductivity. The synthesis of layered multiple-B-cation perovskites provides a considerable challenge because the free-energy difference between ordered and randomly mixed B cations is typically quite small, especially if the size and charge of the cations are similar.[9] In oxygen-deficient compounds, B-cation coordination preferences and ordered oxygen vacancies can be exploited to assist the formation of layered configurations. Requirements for the synthesis of nonstoichiometric mixed-metal layered compounds include B cations that have different coordination preferences and arrangement of vacancies into a specific pattern (usually in $(001)_c$ planes) and A cations that have proper size and coordination preferences.

To take advantage of the ability of copper(II) to adopt 5-fold coordination and in order to achieve B-cation order, we studied systems that, in addition to copper, contained B cations that strongly prefer 6-fold coordination, such as tin(IV), titanium(IV), zirconium(IV), hafnium(IV), and lead(IV) and chose A cations such that the target material would be oxygen deficient. One new quaternary phase found in these systems was $Ba_2La_2Cu_2Sn_2O_{11}$. The compound meets the requirements outlined above for the formation of a nonstoichiometric mixed-metal layered compound, and it contains copper–oxygen and tin–oxygen double layers. As is true of many multiple-cation compounds, such as high-temperature superconductors,[10-16] the structure and crystal chemistry are complex. We report the synthesis and structure of this oxygen-deficient quadruple perovskite. It is the first copper oxide $n = 4$ member of the oxygen-deficient perovskite series $A_nB_nO_{3n-1}$ and, to our knowledge, has a unique vacancy pattern among quadruple perovskites.

Experimental Section

Sample Preparation. $Ba_2La_2Cu_2Sn_2O_{11}$ was prepared by solid-state reaction of the appropriate ratios of barium carbonate (99.99%), lanthanum oxide (99.999%), tin(IV) oxide (99.995+%), and copper(II) oxide (99.999%). The lanthanum oxide was heated in air before use and cooled in a desiccator to remove any traces of water or carbonate. The reagents were ground and fired in high-density alumina boats at 950 °C for 1 day. The sample was quenched in air, ground and pressed into two pellets; one that was less than 1 mm thick and another that was several millimeters thick. The pellets were fired at 1010 °C in air. The thin pellet served a barrier to prevent diffusion of aluminum into the sample.

*To whom correspondence should be addressed.

(1) Murayama, N.; Sudo, E.; Kani, K.; Tsuzuke, A.; Kawakami, S.; Awano, M.; Torii, Y. *Jpn. J. Appl. Phys.* **1988**, *27*, L1623.
(2) Vaughey, J. T.; Wiley, J. B.; Poeppelmeier, K. R. *Z. Anorg. Allg. Chem.* **1991**, *599–600*, 343.
(3) Wiley, J. B.; Markham, L. M.; Vaughey, J. T.; McCarthy, T. J.; Sabat, M.; Hwu, S.-J.; Song, S. N.; Ketterson, J. B.; Poeppelmeier, K. R. In *Chemistry of High Temperature Superconductors II*; Nelson, D. L., George, T. F., Eds.; Symposium Series *377*, American Chemical Society: Washington, DC, 1988; p 304.
(4) Vaughey, J. T.; Thiel, J. P.; Hasty, E. F.; Groenke, D. A.; Stern, C. L.; Poeppelmeier, K. R.; Dabrowski, B.; Hinks, D. G.; Mitchell, A. W. *Chem. Mater.* **1991**, *3*, 935.
(5) Sunshine, S. A.; Schneemeyer, L. F.; Siegrist, T.; Douglass, D. C.; Waszczak, J. V.; Cava, R. J.; Gyorgy, E. M.; Murphy, D. W. *Chem. Mater.* **1989**, *1*, 331.
(6) Huang, Q.; Cava, R. J.; Santoro, A.; Krajewski, J. J.; Peck, W. F. *Physica C* **1992**, *193*, 196.
(7) Er-Rakho, L.; Michel, C.; Lacorre, P.; Raveau, B. *J. Solid State Chem.* **1988**, *73*, 531.
(8) Anderson, M. T.; Poeppelmeier, K. R. *Chem. Mater.* **1991**, *3*, 476.
(9) Patterson, F. K.; Moeller, C. W.; Ward, W. *Inorg. Chem.* **1963**, *2*, 196.
(10) Wu, M. K.; Ashburn, J. R.; Torng, C. J.; Hor, P. H.; Meng, R. L.; Gao, L.; Huang, Z. J.; Wang, Y. Q.; Chu, C. W. *Phys. Rev. Lett.* **1987**, *58*, 908.
(11) Beno, M. A.; Soderholm, D. W.; Capone, D. W.; Jorgensen, J. D.; Schuller, K. I.; Serge, C. U.; Zhang, K.; Grace, J. D. *Appl. Phys. Lett.* **1987**, *51*, 57.
(12) Sheng, Z. Z.; Hermann, A. M. *Nature* **1988**, *332*, 55.
(13) Subramanian, M. A.; Torardi, C. C.; Calabrese, J. C.; Gopalakrishnan, J.; Morrissey, J. J.; Askew, T. R.; Flippen, R. B.; Chowdhry, U.; Sleight, A. W. *Nature* **1988**, *332*, 420.
(14) Chu, C. W.; Bechtold, J.; Gao, L.; Hor, P. H.; Huang, Z. J.; Meng, R. L.; Sun, Y. Y.; Wang, Y. Q.; Xue, Y. Y. *Phys. Rev. Lett.* **1988**, *60*, 941.
(15) Hazen, R. M.; Prewitt, C. T.; Angel, R. J.; Ross, N. L.; Finger, L. W.; Hadidiacos, C. G.; Veblen, D. R.; Heaney, P. J.; Hor, P. H.; Meng, R. L.; Sun, Y. Y.; Wang, Y. Q.; Xue, Y. Y.; Huang, Z. J.; Gao, L.; Bechtold, J.; Chu, C. W. *Phys. Rev. Lett.* **1988**, *60*, 1174.
(16) Cava, R. J.; Batlogg, B.; Krajewski, J. J.; Rupp, L. W.; Schneemeyer, L. F.; Siegrist, T.; vanDover, R. B.; Marsh, P.; Peck, W. F. Jr.; Gallagher, P. K.; Glarum, S. H.; Marshall, J. H.; Farrow, R. C.; Waszczak, J. V.; Hull, R.; Trevor, P. *Nature* **1988**, *336*, 211.

0897-4756/92/2804-1305$03.00/0

The large pellet was quenched, ground, and fired several times in the course of the 7-day reaction period. The sample has to be fired above 990 °C to overcome the stability of $BaSnO_3$. Once formed, the phase is stable at temperatures below 990 °C. Two separate portions of the quenched sample were annealed under flowing oxygen, one at 500 °C and the other at 900 °C. Each was slowly cooled to room temperature.

X-ray Diffraction. A Rigaku diffractometer with nickel-filtered Cu Kα radiation was employed to collect a data set on a quenched polycrystalline sample. A 2θ scan was employed to collect the diffraction data. Data were collected from 5 to 80° with a step of 0.02° in a 10-s collection time at each step. The Bragg peak positions were determined by the use of XRAY-FIT,[17] and the cell constants were refined based on the peak positions by the use of POLSQ.[18] The data set was refined by the use of Rietveld[19] analysis.

Neutron Diffraction. The Intense Pulsed Neutron Source at Argonne National Laboratory was used to collect time-of-flight data on a quenched polycrystalline sample. Data were collected for 4 h on an 11-g sample that was at room temperature and ambient pressure. The d spacing, height, and width of the first 46 peaks ($1.47 \leq d \leq 16.23$ Å) were determined by the use of NUTEFIT,[20] a nonlinear least-squares Marquet method (after Bevington) to fit peaks with a shape function that is the convolution of an exponential rise, an exponential fall, and a Gaussian function. The cell constants were determined and the reflections were indexed by the use of POLSQ.[18] The data from $d = 0.461$ to 2.969 Å were analyzed by Rietveld methods.[21,22] Thirty-seven parameters were refined, which included a scale factor, diffractometer constant, zero-point error, background, peak shape, unit cell and positional parameters, isotropic thermal factors, and absorption and extinction parameters. The coherent scattering lengths[23] used for Ba, La, Cu, Sn, and O were 5.25, 8.24, 7.72, 6.23, and 5.80 fm, respectively.

Electron Microscopy. Polycrystalline samples that had been quenched from 1010 °C were crushed and dispersed onto holey carbon films. Electron diffraction patterns as a function of angle were obtained by the use of a Hitachi 700 microscope operated at 200 kV. The microscope was equipped with a stage that allowed the samples to be tilted ±30°. High-resolution electron microscopy was performed by the use of a Hitachi 9000 microscope operated at 300 kV.

Results

Redox Chemistry. The oxygen content of the copper stannate is 10.98 ± 0.05 based on the average of three thermogravimetric analyses. The reaction is

$$Ba_2La_2Cu_2Sn_2O_{11-\delta} + (4-\delta)H_2 \rightarrow La_2O_3 + Ba_2SnO_4 + Sn^0 + 2\,Cu^0 + (4-\delta)H_2O\uparrow \quad (1)$$

for samples heated 90 min at 1050 °C in an 8.5% H_2/91.5% He atmosphere. The products, except for water vapor, were identified from an X-ray diffraction trace. In addition, the reaction of $BaSnO_3$ under the same conditions results in Ba_2SnO_4, Sn°, and water vapor as determined by X-ray diffraction and mass balance. Within experimental error, the oxygen content calculated from the reduction of $Ba_2La_2Cu_2Sn_2O_{11}$ in hydrogen is consistent with tetravalent tin and divalent copper. ^{119}Sn Mössbauer analysis indicated the tin is exclusively tetravalent. The oxygen content of the samples does not change compared to the quenched sample when treated in flowing oxygen.

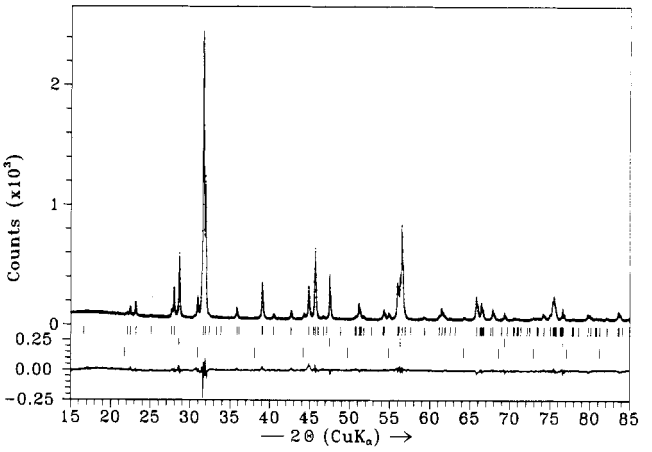

Figure 1. Observed (+), calculated (solid line), and difference (below) X-ray diffraction patterns for $Ba_2La_2Cu_2Sn_2O_{11}$. Tic marks designate possible Bragg reflections for $Ba_2La_2Cu_2Sn_2O_{11}$ (upper), silicon (middle), and $BaSnO_3$ (lower).

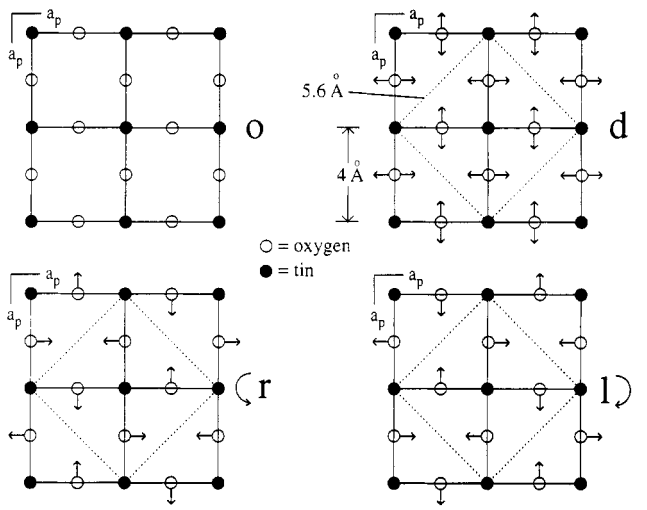

Figure 2. Tin–oxygen nets viewed down [001]. Arrows show displacement of oxygen atoms. The symbols describe the rotations of the SnO_6 polyhedra: o, ordered, no rotations (model 1); d, disordered (models 6, 7); r, right-handed, and l, left-handed (models 2–5). The dotted line outlines the $\sqrt{2}a_p \times \sqrt{2}a_p$ basal plane necessary to maintain 4-fold symmetry.

X-ray Diffraction. $Ba_2La_2Cu_2Sn_2O_{11}$ is tetragonal, has a cell size consistent with a $1a_p \times 1a_p \times 4a_p$ perovskite, and has no systematic absences, which is consistent with extinction symbol P--- and eight possible space groups.[24] Rietveld refinement in space group $P4/mmm$ provides a good model for the refinement of the neutron data; see Figure 1. Table I contains the integrated relative intensities of each of the peaks in the pattern as determined by the use of XRAY-FIT. It was not possible to refine the A-cation distribution owing to the similar atomic numbers of lanthanum and barium.

Neutron Diffraction. Seventeen peaks not detectable in the X-ray experiment are present in the neutron pattern; see Table I. All of the peaks detectable with NUTEFIT[20] can be indexed on a $1a_p \times 1a_p \times 4a_p$ cell. The extinction symbol is P---. Rietveld refinement of the neutron diffraction data in $P4/mmm$ by the use of the model from the X-ray refinement leads to relatively large reliability factors,[25] a thermal factor of 5.58 (1) for the oxygen atom

(17) Thiel, J. P.; Poeppelmeier, K. R. *XRAY-FIT*; Department of Chemistry, Northwestern University, Evanston, IL, 1988.
(18) Kezler, D.; Ibers, J. A. *Modified POLSQ*; Department of Chemistry, Northwestern University, Evanston, IL, 1983.
(19) Wiles, D. B.; Sakthivel, A.; Young, R. A. *Rietveld Analysis Program DBWS-9006PC*; School of Physics, Georgia Institute of Technology, 1990.
(20) Thiel, J. T.; Poeppelmeier, K. R. *NUTEFIT*; unpublished FORTRAN program to fit neutron data, 1991.
(21) Von Dreele, R. B.; Jorgensen, J. D.; Windsor, C. G. *J. Appl. Crystallogr.* **1982**, *15*, 581.
(22) Rotella, F. J.; Richardson, J. W. Jr. *Workshop on Neutron Scattering Data Analysis 1986*; IOP: Bristol, UK, 1986; Chapter 1.
(23) Jacobson, A. J.; Tofield, B. C.; Fender, B. E. F. *J. Phys. C* **1973**, *6*, 1615.
(24) In *International Tables for Crystallography*; Hahn, T., Ed.; D. Reidel: Boston, 1983; Vol. A, p 45.

Table I. Indexed Neutron Diffraction Pattern for $Ba_2La_2Cu_2Sn_2O_{11}$ and Relative Intensities from Neutron and X-ray Diffraction Data[a]

h k l	d_{calc}, Å	d_{obs},[b] Å	I_{rel} (ND)	I/I_0 (XRD)
0 0 1	16.2314			
0 0 2	8.1157	8.1174	0.4	0.3
0 0 3	5.4105			
		4.1160*	0.2	
0 0 4	4.0579	4.0617	2	1
1 0 0	3.9891	3.9934	2	2
1 0 1	3.8739	3.8747	0.1	3
1 0 2	3.5800	3.5814	1	
0 0 5	3.2463	3.2483	0.4	4
1 0 3	3.2108			10
		2.9079*	0.3	9
1 0 4	2.8447	2.8443	17	100
1 1 0	2.8207	2.8206	7	34
1 1 1	2.7791	2.7788	0.3	
0 0 6	2.7052	2.7051	3	
1 1 2	2.6644	2.6640	1	
1 0 5	2.5179	2.5176	9	4
1 1 3	2.5012	2.5010	4	
		2.3737*	3	
0 0 7 }	2.3188	2.3161	57	25
1 1 4 }	2.3161			
1 0 6	2.2390	2.2387	7	2
1 1 5	2.1292	2.1364	1	3
		2.0555*	5	3
0 0 8	2.2089	2.0286	27	30
1 0 7	2.0047			
2 0 0	1.9946	1.9943	100	30
2 0 1	1.9797	1.9812	3	
1 1 6	1.9525	1.9522	9	1
2 0 2	1.9369	1.9367	3	
2 0 3	1.8715	1.8690	0.5	
		1.8389*	1	
1 0 8 }	1.8085	1.8078	7	1
0 0 9 }	1.8035			
1 1 7 }	1.7912	1.7899	8	
2 0 4 }	1.7900			
2 1 0	1.7840	1.7839	8	
2 1 1	1.7733	1.7733	2	0.9
2 1 2	1.7424	1.7422	2	
2 0 5	1.6994	1.6994	3	
2 1 3	1.6943	1.6947	1	6
		1.6785*	1	6
1 1 8 }	1.6471	1.6469	28	16
1 0 9 }	1.6434			
2 1 4	1.6331	1.6329	66	12
0 0 10	1.6231	1.6232	11	
2 0 6	1.6054	1.6052	12	
2 1 5	1.5635	1.5632	9	1
1 1 9	1.5195	1.5199	3	3
2 0 7	1.5121	1.5120	31	5
1 0 10	1.5035	1.5038	3	4
2 1 6	1.4893	1.4891	16	1
0 0 11	1.4756	1.4755	2	

[a] Note: * designates $BaSnO_3$ reflection. The neutron d spacings and relative intensities were determined with NUTEFIT, and the X-ray diffraction relative intensities were determined with XRAY-FIT. [b] d spacings from neutron diffraction are similar to those from X-ray diffraction as shown by the similarity of cell constants that were determined from least-squares analysis of the d spacings; a = 3.9891 (3) Å and c = 16.231 (1) Å from neutron data, a = 3.9868 (2) Å and c = 16.224 (1) Å from X-ray data.

in the tin–oxygen plane, O2, and severe undercalculation of the intensity of the *hl4* reflections ($h > 0$); see model 1 in Table II. Each of the problems is alleviated by displacements of the oxygen atoms in the tin-oxygen plane,

(25) $R_{profile} \equiv 100\sum[|(Y_{obs} - Y_{calc})|]/\sum[|(Y_{obs})|]$; $R_{weighted\ profile} \equiv 100(\Sigma[W*(Y_{obs} - Y_{calc})^2])^{1/2}/\sum[W(Y_{obs})^2])^{1/2}/\sum[W(Y_{obs})^2])$; $R_{|F|^2} \equiv 100\sum[|(I_{obs} - I_{calc})|]/\sum[|(I_{obs})|]$; $R_{Rietveld} \equiv 100\sum[|(Y_{obs} - Y_{calc})|]/\sum[|(Y_{obs}) - background|]$; $R_{expected} \equiv 100$ (number of degrees of freedom/$\sum[W(Y_{obs})^2])^{1/2}$. Y_{obs} and Y_{calc} are the observed and calculated profile intensities at a particular time-of-flight value, respectively, and W is $1/Y_{obs}$. I_{obs} and I_{calc} are the observed and calculated intensities of each Bragg peak, respectively.

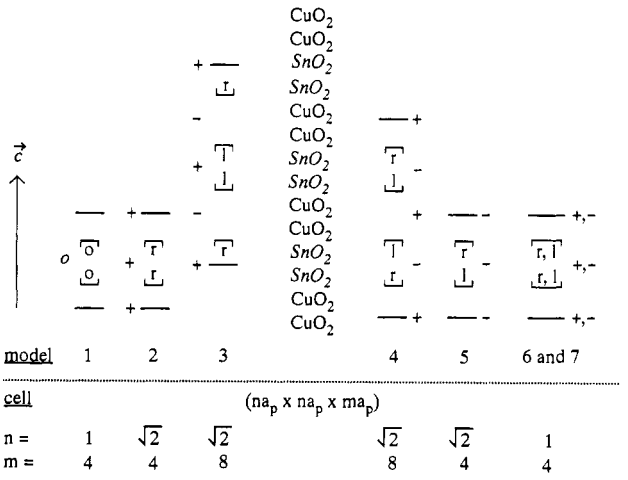

Figure 3. Schematic of cell size (solid lines) and rotation pattern for models one through seven. The cell size relative to cubic perovskite is listed below. The sense of the rotations within [ ] and between] [double layers is indicated by plus (+) if the sense is the same, minus (–) if it is opposite, plus, minus (+, –) if there is no correlation, and zero (0) if there are no rotations. n and m are not related to n_i and m_j used later.

that is, rotations of the SnO_6 octahedra around [001].

The rotations of the SnO_6 octahedra within each tin–oxygen layer can be right-handed (r), left-handed (l), or disordered (r,l) as viewed down [001]; see Figure 2. The sense of the rotations parallel to [001] can be completely correlated (greater than 1000 Å; models 2–5), not correlated at all (models 6 and 7), or correlated over a short range (50–1000 Å, discussed later). The cell sizes for each model, a depiction of the rotation patterns, and the labels for the tilt notation (+, –, or 0) are presented in Figure 3. The tilt notation used in Table II was first introduced by Glazer.[26] The letters designate the relative magnitude of the tilt above a given axis, and the superscripts designate the relative sense of the tilts from layer to layer. Within each tin–oxygen double layer, the sense of the rotations (designated by the first superscipt) is either the same from layer to layer, labeled plus (+), or the opposite, labeled minus (–). From double layer to double layer, the sense of the rotations (designated by the second superscript) is either the same across the interface (+) or the opposite (–). If there are no rotations about a particular axis, the label is zero (0).

Table II shows that the models with complete correlation of the SnO_6 rotations (2–5) provide significant improvement over the model with no rotations of the SnO_6 octahedra (model 1). However, the models with no correlation of the SnO_6 rotations (6 and 7), are superior to the models that have complete correlation (2–5) because they (1) provide a better fit, in particular, to the *hl4* reflections (2) provide lower R values (3) have lower thermal factors for O2. However, as presented below, the models with no correlation (6, 7) do not fully describe the long-range structure.

Electron Microscopy. Within a tetragonal crystal system, rotations of the SnO_6 octahedra require a $\sqrt{2}a_p \times \sqrt{2}a_p$ expansion of the basal plane to maintain fourfold symmetry, see Figure 2. Electron diffraction patterns in the [001] zone show clear evidence of the $\sqrt{2}a_p \times \sqrt{2}a_p$ basal plane, which confirms that the SnO_6 octahedra are

(26) Glazer, A. M. *Acta Crystallogr., Sect. B* **1972**, *28*, 3384.

(27) For a general description of the terminology used in this paper see: *High-Resolution Transmission Electron Microscopy and Associated Techniques*; Buseck, P. R., Cowley, J. M., Eyring, L., Eds.; Oxford: New York, 1988; pp 340–342.

Table II. Models Used for Neutron Refinement

model	tilt notation[a]	space group	no. of variables	R_p[b]	R_{wp}	R_I	R_{Riet}	B O2
1	$a^0a^0c^0$	$P4/mmm$	35	7.3	10.7	13.3	17.1	5.6
2	$a^0a^0c^{++}$	$P4/mbm$	37	6.5	8.0	10.9	14.5	3.3
3	$a^0a^0c^{+-}$	$I4/mcm$	37	6.8	10.0	20.5	15.6	3.7
4	$a^0a^0c^{-+}$	$I4/mcm$	37	6.4	9.4	19.5	14.7	3.0
5	$a^0a^0c^{--}$	$P4bm$	52	6.0	8.8	8.5	12.9	5.4/0.9
6	$a^0a^0c^{\pm}$	$P4/mmm$	37	5.5	8.0	10.3	12.6	1.7
7	$a^0a^0c^{\pm}$	$P4mm$	52	5.0	7.4	8.6	11.0	1.3/0.6

[a] In this modified Glazer notation, the first sign indicates the relative sense of the rotations *within* the tin-oxygen double layers and the second indicates the relative sense of the rotations from *double layer to double layer*; see text. [b] $R_{expected}$ = 2.8% for all models.

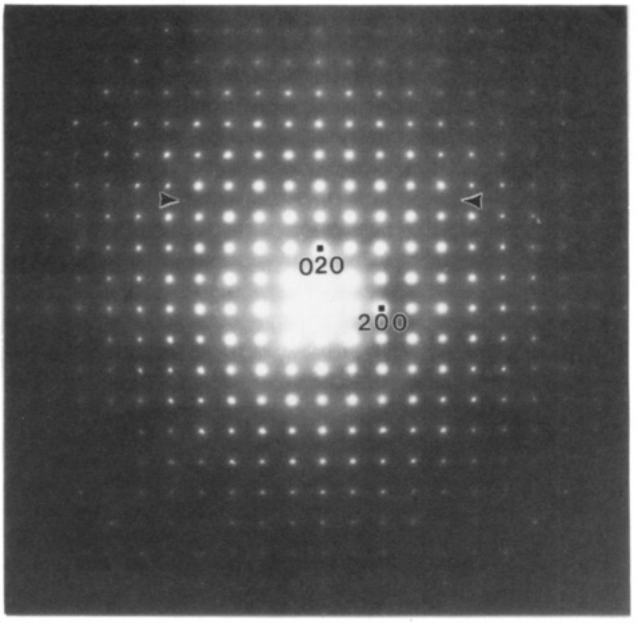

Figure 4. Electron diffraction pattern obtained from [001] zone. Weak spots at $p/2$ ⟨110⟩, p = 1, 3, 5, 7, ..., indicate the basal plane is $\sqrt{2}a_p \times \sqrt{2}a_p$ and that the SnO_6 polyhedra are rotated around [001].

rotated; see Figure 4. High-resolution transmission electron microscopy from the [100] zone verifies the $4a_p$ subcell along [001]; see Figure 5. Electron diffraction patterns from [100] to [110] zones obtained by rotation around [001] show that as a single crystallite is tilted it exhibits extra reflections and streaks along the line g = $^1/_2(130)$ + $(00l)$ in the [310] zone; see Figure 6. The extra reflections are consistent with short-range correlation of the sense of the SnO_6 rotations. The extra spots were observed in several crystallites and are believed to be a common feature. Figure 7 shows that there are 24 maxima and minima from one node n_i to the next n_{i+1} and 24 from one maximum m_j to the next m_{j+1}. The extra spots g' = $^1/_2(130)$ + $(00l')$, where $(00l')$ = $l'/6(001)$ and l' = 1, 3, 5, ..., indicate the presence of a commensurate superlattice that is $24a_p$ ($6 \times c_{subcell}$) along [001] in real space.

The superlattice gives rise to intensity in the form of several extremely broad peaks in the neutron diffraction pattern (from node to node the peaks are at least 0.38 Å wide); see the inset in Figure 8. Each diffuse peak n_i to n_{i+1} in the neutron pattern is an envelope of several peaks and contains contributions to its intensity from the g' = $^1/_2(130)$ + $(00l')$ reflections. The positions and widths (node to node) of the neutron peaks can be calculated from the g spacings of the electron diffraction experiment. The g spacings are calculated from the law of cosines (in this special case the Pythagorean relation) from eq 2, where, by visual inspection, l_{ni} appears to be nearly equivalent to

$$g_{ni}^2 = (1/2d_{310})^2 + (l_{ni}/16.23)^2 \qquad (2)$$

Table III. Positions of the Minima and Maxima from Superlattice Diffraction

i,j	1	2	3	error
g_{ni} (Å)	2.52	2.14	1.60	±0.05
g_{mj} (Å)	2.41	1.93	1.41	±>0.05

l in $\vec{c}$, and 16.23 is the c-axis length in angstroms. The minima and maxima are listed in Table III. The broad peak between n_1 and n_2 has a maximum intensity of about 50 counts (about 0.4% counts/maximum counts) in the neutron pattern and is about 0.38 Å wide. The integrated intensity is substantial (roughly 10% I/I_0). The intensity of the peaks between n_i and n_{i+1}, $i \geq 2$, is weaker than the peak between n_1 and n_2, as in the electron diffraction experiment, and the $i \geq 2$ peaks are not obvious in the neutron pattern. The presence of the broad peaks between n_i and n_{i+1}, i = 1, 2 in the neutron experiment confirms that the $24a_p$ modulation period is indeed a common feature of the crystallites.

There is a broad Bragg peak at 1.37 Å centered near the calculated maximum m_3 in the neutron pattern that is observed but not calculated by any model 1–7. This peak may be caused by the $6 \times c_{subcell}$ ($24a_p$) superlattice, some other aspect of the short-range order that was not modeled in the neutron diffraction analysis, or by an unidentified impurity.

Description of Structure. The average structure of $Ba_2La_2Cu_2Sn_2O_{11}$ is described by a $1a_p \times 1a_p \times 4a_p$ subcell that contains a statistical distribution of the oxygen atoms in the tin–oxygen layers, O2, over an 8t site (and a statistical distribution of the oxygen atoms in the copper–oxygen layers, O4, over a different 8t site), models 6 and 7. Model 6 is judged superior to model 7 because it has fewer structural variables (17 versus 31) and all of the temperature factors are positive. The observed, calculated and difference patterns along with the allowed reflections for model 6 are displayed in Figure 8. The overall fit is acceptable but reflects the inability to model the effects of short-range correlation of the SnO_6 rotations. Note that the difference in coherent scattering lengths allowed the refinement of the distribution of lanthanum and barium cations. The atomic parameters for model 6 appear in Table IV. A polyhedral representation of the structure is shown in Figure 9.

Electron diffraction indicates (1) the $1a_p \times 1a_p \times 4a_p$ subcell cannot describe all of the long-range structural information, that is, the structure is modulated,[27] and (2) the modulations are commensurate with a dominant superlattice of $\sqrt{2}a_p \times \sqrt{2}a_p \times 24a_p$. No attempt has been made to model the structure based on the 5.5 × 5.5 × 97 Å supercell. Such a model would have to account for the strong diffraction from and the uniqueness of the [310] zone and the diffuse peaks in the neutron pattern.

The similarity of the stannate to $Tl_2Ba_2Ca_1Cu_2O_8$[12,13] (2212) can be seen when it is written $Sn_2(Ba_2La)LaCu_2O_{11}$ (2312). The thallium compound has a sequence of Ca□ CuO_2 BaO [TlO TlO] BaO CuO_2 Ca□ perpendicular to c,

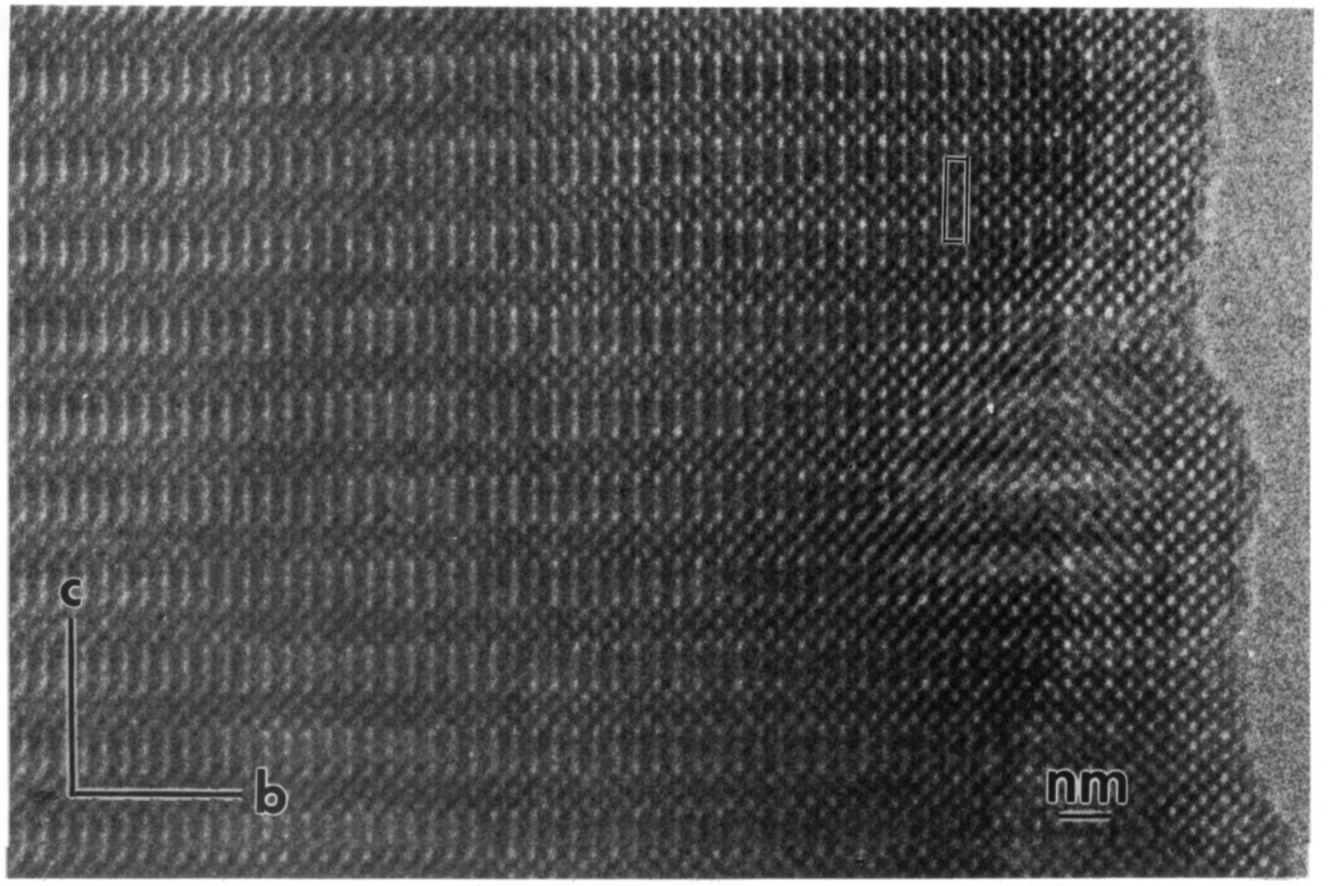

Figure 5. High-resolution image obtained from the [100] zone. The 16.23-Å cell is outlined.

Table IV. Atomic Parameters for $Ba_2La_2Cu_2Sn_2O_{11}$[a]

atom	site	x/a (σx)	y/b (σy)	z/c (σz)	B (Å²) (σB)	occupancy
La1	1c	1/2	1/2	0	0.53 (5)	1[b]
La2/Ba2	2h	1/2	1/2	0.2244 (1)	0.92 (5)	0.14/0.86 (2)
La3/Ba3	1d	1/2	1/2	1/2	0.55 (4)	0.72/0.28 (2)
Cu	2g	0	0	0.1097 (1)	0.34 (3)	1
Sn	2g	0	0	0.3693 (1)	0.16 (3)	1
O1	1b	0	0	1/2	2.20 (8)	1
O2	8t	0.0894 (6)	1/2	0.3811 (2)	1.67 (5)	1/2
O3	2g	0	0	0.2466 (2)	1.82 (5)	1
O4	8t	0.0170 (18)	1/2	0.0967 (1)	0.52 (4)	1/2
O5v	1a	0	0	0		0[c]

[a] Model six, space group $P4/mmm$ and a = 3.9893 (3), c = 16.232 (1) Å, and Z = 1. [b] Value refined to La2/Ba2 = 0.98/0.02 (2) and was set to value above in final refinement. [c] Value refined to 0.00 (2) and was set to zero in final refinement.

whereas the tin compound has a sequence La□ CuO_2 BaO [SnO_2 LaO SnO_2]BaO CuO_2 La□ perpendicular to c. The thallium–oxygen octahedra share edges and the tin–oxygen octahedra share corners.

Properties. Magnetic susceptibility measurements from 5 to 300 K on a quenched sample display a broad maximum above 300 K consistent with two-dimensional antiferromagnetic order. The material is a semiconductor and has a room temperature resistance of about 2000 Ω cm. A sample that was previously slowly cooled from 500 °C in oxygen exhibits a diamagnetic signal below 30 K. The transition is broad and the shielding fraction is less than 0.1%. A very small impurity (less than 2% I/I_0) is present in the X-ray diffraction pattern. The impurity has a diffraction pattern similar to La_2CuO_4. On the basis of the diffraction pattern of the impurity and the 30 K transition temperature, it is assumed that $La_{2-x}Ba_xCuO_4$ is responsible for the diamagnetic signal. Under the synthesis conditions reported, $Ba_2La_2Cu_2Sn_2O_{11}$ appears to be a point compound. Attempts to dope it p-type with barium, strontium, or calcium for lanthanum or n-type with cerium for lanthanum have produced a mixture of phases.

Discussion

Synthetic Strategy. There are several examples of cuprates that contain two B cations and employ ordered oxygen vacancies to achieve a layered structure. Compounds include $Ba_2LaCu_2TaO_8$,[1,28,29] $LaSrCuTO_5$ (T = Ga,[2,30] Al[3]), $LnSr_2Cu_2TO_7$ (T = Ga[4], Al,[5,31] Fe, Co[6]), and $YBaCuFeO_5$.[7,32-34] The important aspects to consider

(28) Greaves, C.; Slater, P. R. *Physica C* **1989**, *161*, 245.
(29) Rey, M.-J.; Dehaudt, Ph.; Joubert, J.; Hewat, A. W. *Physica C* **1990**, *167*, 162.
(30) Vaughey, J. T.; Shumaker, R.; Song, S. N.; Ketterson, J. B.; Poeppelmeier, K. R. *Mol. Cryst. Liq. Cryst.* **1990**, *184*, 335.
(31) Slater, P. R.; Greaves, C. *Physica C* **1991**, *180*, 299.
(32) Mayer, C.; Hartmann-Boutron, F.; Gros, Y.; Strobel, P. *Solid State Commun.* **1990**, *76*, 163.
(33) Pissas, M.; Mitros, C.; Kallias, G.; Psycharis, V.; Niarchos, D.; Simopoulos, A.; Kostikas, A.; Christides, C.; Prassides, K. *Physica C* **1991**, *185–189*, 533.

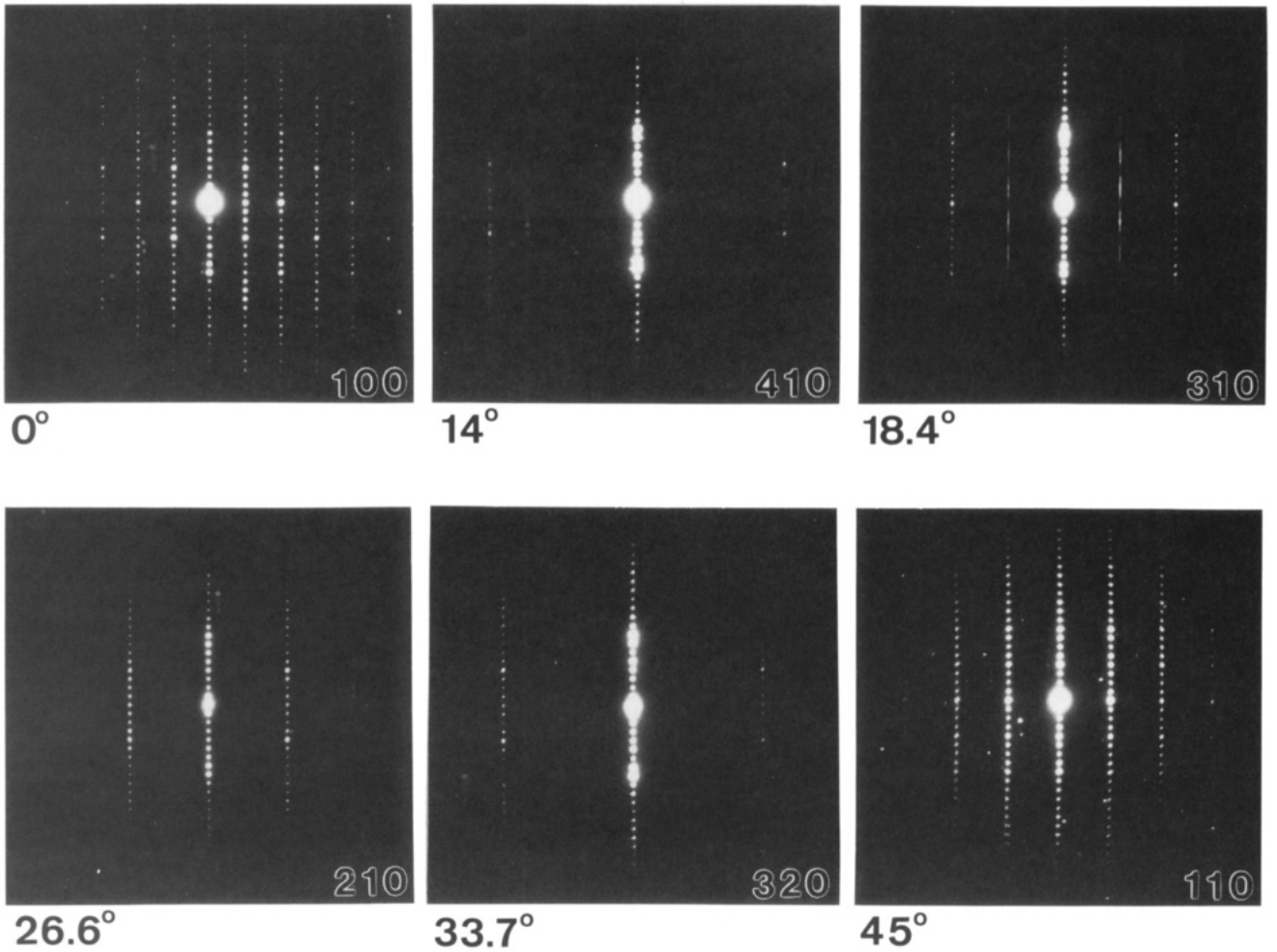

Figure 6. Electron diffraction patterns obtained as a single grain was tilted from [100] to [110] around the tilt axis [001]. Numbers at the lower right indicate the zone, and numbers at the lower left indicate the rotation angle about [001].

when one targets new oxygen-deficient mixed-metal cuprates are the desired coordination environments for copper[35] and the other B cation (the environments should be different), the copper-to-B-cation ratio, the number of vacancies needed per formula unit, and the size and charge of the A cations.

The structure of $Ba_2La_2Cu_2Sn_2O_{11}$ illustrates how ordered vacancies can be incorporated to produce layered structures. Two copper atoms share each oxygen vacancy and form CuO_5–□–CuO_5 units parallel to [001]. The vacancies order in (001) A□$_{4/4}$ planes (the first four indicates the number of vacant perovskite oxygen sites around each A cation and the second four indicates the number of A cations around each vacant oxygen site) and provide double copper–oxygen layers and square pyramidal copper. A statistical distribution of B cations is avoided because tin(IV) strongly prefers octahedral coordination. The tin atoms form corner-shared double-octahedral slabs that interleave the copper–oxygen layers.

Copper–Tin Size Mismatch. The physical explanation for the modulated structure is related to the size difference of copper and tin. There is a severe mismatch across the interface of the copper–oxygen and tin–oxygen nets.[36] The mismatch is two-dimensional and places the longer Sn–O bonds under compression[37] and the shorter Cu–O bonds under tension. The mismatch is partly relieved by rotation of the tin–oxygen octahedra; see Table V for rotation angles. The correlation of the sense of the SnO_6 rotations is about 97 Å parallel to [001]. The modulated structure is characteristic of the correlation of the SnO_6 rotations and/or other structural modifications, such as displace-

Table V. Bond Distances[a] and Angles for $Ba_2La_2Cu_2Sn_2O_{11}$[b]

Bond Distances			
La1–O4	2.486 (4) × 4	Cu–O4	2.007 (1) × 4
–O4	2.592 (4) × 4	–O3	2.222 (3)
La2–O4	2.830 (5) × 2	Sn–O3	1.998 (4)
–O3	2.843 (5) × 4	–O2	2.035 (1) × 4
–O4	2.925 (1) × 2	–O1	2.115 (2)
–O2	3.026 (3) × 2		
–O2	3.464 (3) × 2		
La3–O2	2.531 (2) × 4		
–O1	2.821 (1) × 4		
–O2	3.041 (2) × 4		
Bond Angles[c]			
O4–Cu–O4	89.36 (1)	O2–Sn–O2	89.52 (2)
O3–Cu–O4	96.04 (7)	O1–Sn–O1	84.77 (9)
Cu–O4–Cu	167.3 (5)	Sn–O2–Sn	157.1 (5)
Rotation Angles			
Cu–Cu–O4	1.9 (4)	Sn–Sn–O2	10.1 (1)

[a] For oxygen atoms within 3.5 Å. [b] Bond distances in angstroms, and bond angles in degrees. [c] For oxygen atoms with the same sense of rotation about [001].

(34) Vaughey, J. V.; Poeppelmeier, K. R. *NIST Pub. 804, Proceedings of the International Conference on Chemistry of Electronic Ceramic Materials*; Davies, P. K., Roth, R. S., Eds.; U.S. Government Printing Office: Washington, DC, 1991; pp 419–426.

(35) Copper(II) is known in six (elongated octahedral), five (square pyramidal and trigonal bipyramidal), and four (square planar and tetrahedral) coordination.

(36) A common copper–copper distance within a $CuO_{4/2}$ layer is 3.8 Å. A common tin–tin distance within a $SnO_{4/2}$ layer is 4.1 Å.

(37) Brisse, F.; Knop, O. *Can. J. Chem.* **1968**, *46*, 859.

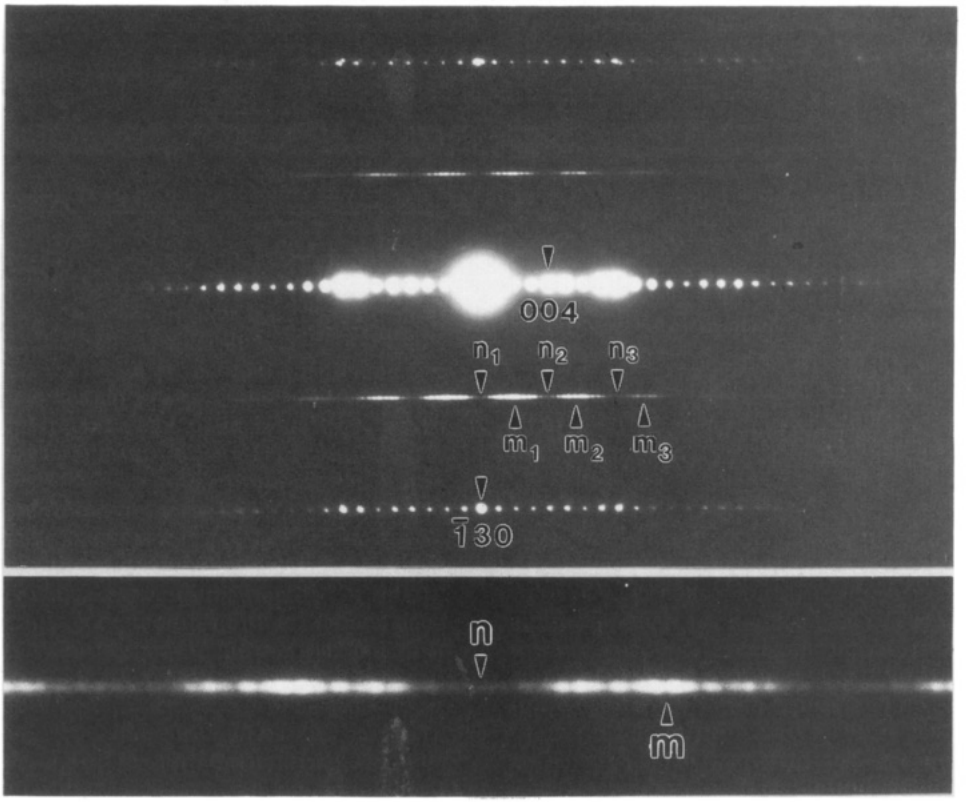

Figure 7. Electron diffraction pattern from the [310] zone. Extra reflections occur at $g = {}^1/_2(130) + (00l)$. n_i and m_j ($i, j = 1, 2, 3, \ldots$) mark the maximum and minimum intensities of the 24 reflections from n_i to n_{i+1} or m_j to m_{j+1}. An expanded view of the $g = {}^1/_2(130) + (00l)$ reflections is shown below.

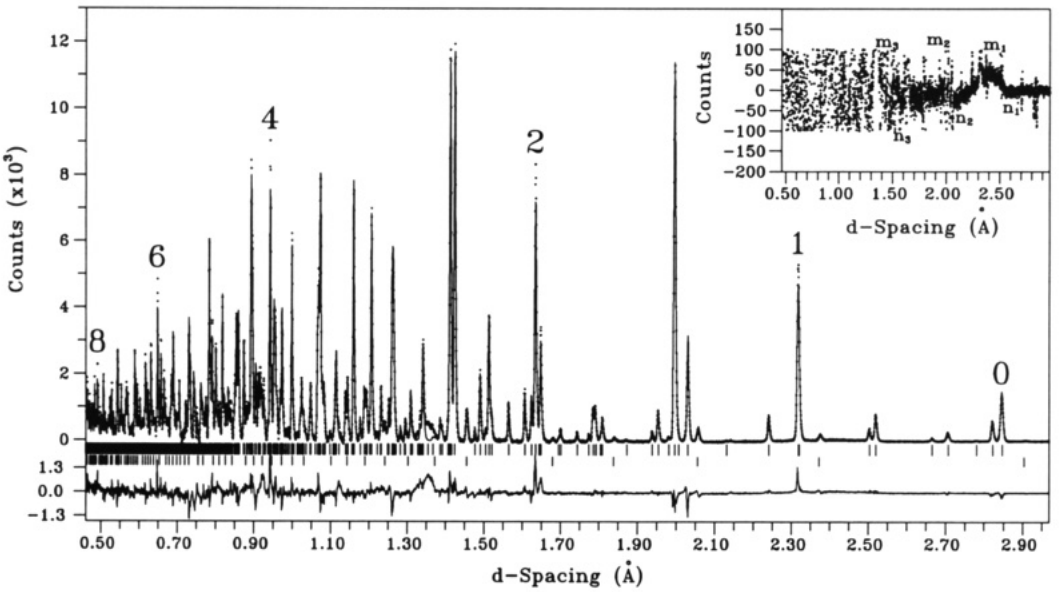

Figure 8. Observed (+), calculated (solid line), and difference (below) neutron diffraction patterns for $Ba_2La_2Cu_2Sn_2O_{11}$. Numbers refer to h of an $hl4$ reflection. Tic marks designate possible Bragg reflections for $Ba_2La_2Cu_2Sn_2O_{11}$ (upper) and $BaSnO_3$ (lower). Inset shows an expanded view of the difference pattern. Differences greater than 100 counts are clipped. Note the prominent diffuse peak between n_1 and n_2.

ments of the A cations, the rotations cause. The structure might show correlation of the rotations over distances longer than 100 Å if single crystals can be grown or if the microstructure can be controlled with thermal or chemical treatments. In these cases, one of the models 2–5 would likely describe the structure, and the physical properties might be significantly affected.

As a result of the copper–tin size mismatch, the in-plane copper–oxygen bond length is 2.007 (1) Å, which is about 0.04–0.10 Å longer than in high-temperature cuprate superconductors. For example, the in-plane bond lengths for $YBa_2Cu_3O_{6.81}$[11] are 1.928 (1) and 1.962 (1) Å. The axial copper–oxygen bond length in $Ba_2La_2Cu_2Sn_2O_{11}$ is long owing to a Jahn–Teller distortion, just as in $YBa_2Cu_3O_{6.81}$. Bond distances and angles are shown in Table V.

A-Cation Order. The A cations are ordered. Lanthanum occupies the eight-coordinate site between the copper–oxygen planes. In addition, lanthanum preferentially (72/28) occupies the 12-coordinate site between the tin–oxygen planes. Barium preferentially (86/14) occupies the 12-coordinate site between the copper–oxygen and tin–oxygen planes. The tetravalent tin atoms are displaced

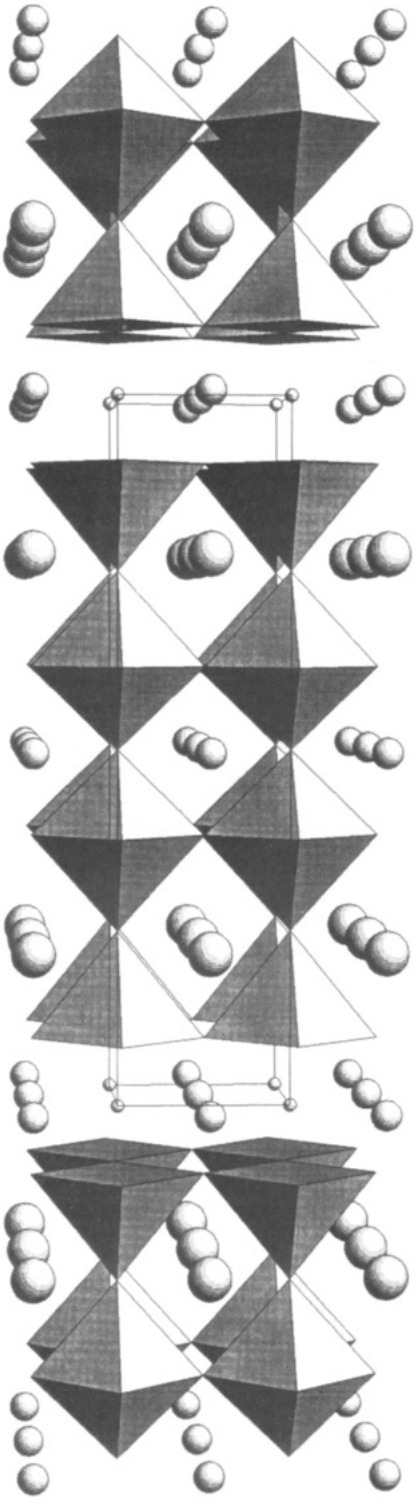

Figure 9. Polyhedral representation of the structure of $Ba_2La_2Cu_2Sn_2O_{11}$ viewed down [100]. The octahedra are SnO_6, pyramids are CuO_5, largest spheres are barium sites, medium spheres are lanthanum sites, and smallest spheres are oxygen vacancies. The disorder associated with oxygen atoms O2 and O4 is not shown.

away from the site preferentially occupied by lanthanum, La2/Ba2 (formal charge +2.72), toward the site preferentially occupied by barium, La3/Ba3 (formal charge +2.14). All of the in-plane oxide ions that are bonded to tin and copper are displaced toward the more highly charged A-cation sites (La1 and La2). The complex crystal chemistry leads to buckled tin–oxygen and copper–oxygen planes and causes the Sn–O2–Sn (157.1° (5)) and Cu–O4–Cu (167.3° (5)) angles to deviate from the linear value of 180°. The copper–copper distance from one $CuO_{4/2}$ layer to the one directly above or below it is 3.56 Å, which opens the possibility for incorporation of oxygen between the layers; however, no excess oxygen is detected by thermogravimetric analysis of quenched samples or samples slowly cooled in flowing oxygen.

Tin–Oxygen Double Layers. The tin–oxygen double layers are an interesting and unexpected features of this material. Several examples are known where the chain copper of $YBa_2Cu_3O_7$ has been replaced with another metal atom,[1-6] but all have single M–O layers. In compounds such as $Ba_2LaCu_2MO_8$ (M = Nb, Ta)[1,28,29] and the present compound, the A-cation site between the $CuO_{4/2}/MO_{4/2}$ interface is abnormally large owing to the size of the M ion and the long apical copper–oxygen bond. In all the compounds, the site is occupied by barium. In general, it appears that when B cations larger than copper are present an ion significantly larger than lanthanum (1.34 Å), such as barium (1.51 Å), is required between the Cu–O and M–O layers to stabilize the structure. In the present compound, the additional tin–oxygen layer is necessary in order to have one barium per copper and maintain electroneutrality and proper oxygen content. To underscore the need for a large A cation, we point out that for the stannate to have single M–O layers and one oxygen vacancy per unit cell, the composition would have to be "$BaLa_2Cu_2SnO_8$" and a significant amount of lanthanum would reside on the A-cation site between the copper–oxygen/tin–oxygen layers. A sample prepared at this composition is a mixture of phases, predominantly $BaSnO_3$, $Ba_2La_2Cu_2Sn_2O_{11}$, and a La–Ba–Cu–O (214-type) phase. For mass balance there must be a copper-rich phase such as CuO present, but none was positively identified. In addition, the phases "$M_2La_2Cu_2Sn_2O_{11}$" do not form with alkaline-earth M atoms smaller than barium, such as strontium and calcium.

Structure–Property Relationships. The structure–property relationships in the double-layer compound $Ba_2La_2Cu_2Sn_2O_{11}$ ($BaLaCuSnO_{5.50}$) are likely similar to those in the single-layer compound La_2CuSnO_6.[8] Both compounds have an anisotropic (i.e., layered) distribution of B cations and are characterized by a severe mismatch across the $SnO_{4/2}/CuO_{4/2}$ interface. In both compounds, the mismatch causes the SnO_6 octahedra to rotate, stretches the copper–oxygen bond lengths (1.99 Å average in the single-layer compound, 2.00 Å average in the double-layer compound) and buckles the copper–oxygen planes (157–165° and 167°, respectively). When La_2CuSnO_6 is oxidized, i.e., $La_{2-x}Ba_xCuSnO_6$ ($0.00 \leq x \leq 0.15$), the compound remains an antiferromagnetic semiconductor.[38] The inability to make $La_{2-x}Ba_xCuSnO_6$ a superconductor most likely results from the long in-plane copper–oxygen bond lengths, which provide poor overlap of the Cu $d_{x^2-y^2}$ and O 2p orbitals. In contrast to La_2CuSnO_6, we have not been able to incorporate dopants to oxidize $Ba_2La_2Cu_2SnO_{11}$. If the compound can be oxidized, the electronic behavior of the copper–oxygen planes is expected to be similar to $La_{2-x}Sr_xCuSnO_6$. If either compound can be reduced, the structure–property relationships may be different owing to the long in-plane copper–oxygen bond lengths, which may be favorable for n-type superconductivity.

Conclusions

In mixed-metal oxides, ordered oxygen vacancies coupled with a difference in cation coordination preferences

(38) Anderson, M. T.; Poeppelmeier, K. R.; Gramsch, S. A.; Burdett, J. K. *J. Solid State Chem.*, in press.

can be employed to control the formation of two-dimensional features in three-dimensional structures. $Ba_2La_2Cu_2Sn_2O_{11}$ and other multication compounds such as high-temperature superconductors adopt a common and relatively simple structure type (perovskite), but their crystal chemistry is complex and leads to complicated distortions of the basic structure. The nature of the distortions and their effect on the structure and solid-state chemistry must be understood in order to control and ultimately understand their electronic and other physical properties. Superconductivity may be possible in $Ba_2La_2Cu_2Sn_2O_{11}$ provided several factors can be addressed and overcome, such as the inability to chemically oxidize or reduce the compound, the diminished overlap of the copper $d_{x^2-y^2}$ and oxygen 2p orbitals, and the control of the microstructure by thermal or chemical treatments.

Acknowledgment. This work benefitted from the use of the Intense Pulsed Neutron Source at Argonne National Laboratory with funding provided by the National Science Foundation and the Science and Technology Center for Superconductivity (NSF-DMR-8809854). The authors thank R. Hitterman and J. Richardson for their assistance with the neutron diffraction experiment. We gratefully acknowledge J. P. Thiel and J. T. Vaughey for helpful discussions. We also acknowledge the Northwestern Materials Research Center for support of the X-ray Diffraction Facility (MRL-DMR-8821571).

Registry No. $Ba_2La_2Cu_2Sn_2O_{11}$, 144224-60-2.

High-Temperature Chemistry of the Conversion of Siloxanes to Silicon Carbide

Gary T. Burns,† Richard B. Taylor,† Youren Xu,‡ Avigdor Zangvil,‡ and Gregg A. Zank*,†

Dow Corning Corporation, Midland, Michigan 48686-0995, and Materials Research Laboratory, University of Illinois at Urbana—Champaign, Urbana, Illinois 61801

Received June 12, 1992. Revised Manuscript Received August 7, 1992

The preparation of siloxane polymers as precursors to silicon carbide has been investigated. To make these polymers useful as binder materials for ceramic powders in the preparation of dense (sintered) ceramic monoliths, methods were developed to control the silicon carbide to carbon ratios in the polymer derived ceramic. Insights into the chemistry of the conversion of these high oxygen polymers to silicon carbide ceramics were obtained by following the pyrolysis products by elemental analysis, quantitative X-ray diffraction, ^{29}Si MAS NMR spectroscopy, Raman spectroscopy, and transmission electron microscopy. The pyrolysis proceeds by the formation of an amorphous SiCO material at 1200 °C that continues to undergo an Si–O for Si–C bond redistribution so that trace amounts of β-SiC are seen at 1400 °C. By 1600 °C the carbothermic reduction is well underway with only a small percentage of oxygen remaining in the material. At 1800 °C the pyrolysis is complete. The final ceramic is composed of substantial amounts of crystalline β-SiC and excess carbon that is present as turbostratic graphite.

Introduction

Since the discovery of polycarbosilane by Yajima[1] and its subsequent demonstration as a silicon carbide precursor, a variety of polymeric precursors to silicon carbide have been prepared.[2] While these polymeric precursors represent synthetic accomplishments, they also present a variety of challenges for the polymers to be of true ceramic utility. The majority of these polymers were developed to "simplify" the fabrication of ceramic films, fibers, composites, and monoliths. Currently shaped ceramic parts are made by die pressing, injection, and resin transfer molding, composite reinfiltration and extrusion processes that employ fugitive binders. Unfortunately, few of the published polymeric routes to ceramics have the synthetic versatility to tailor the polymer's rheology, cure chemistry, and ceramic composition to the fabrication process required to make a ceramic article.

Within our laboratories we have been investigating a variety of preceramic polymers that would be suitable as binders for the sintering of SiC powders.[3-5] Since 1953 several literature reports have surfaced that detail the requirements for pressureless sintering of SiC monoliths:[6] (1) high-purity submicron spherical powder; (2) the presence of 0.3–2 wt % added carbon; (3) a sintering aid, which is most commonly boron or aluminum; (4) processing to high temperatures, generally above 2000 °C. On the basis of these requirements, we have attempted to prepare polymers that not only function to bind the powders together but also decompose by temperatures of 2000 °C to add sufficient amounts of carbon for densification and additional silicon carbide to reduce the overall shrinkage associated with the sintering process.

Siloxanes and silsesquioxane sol–gels have been prepared and touted as useful in a variety of ceramic applications such as precursors to powders: silicon oxynitride,[7] silicon

† Dow Corning Corp.
‡ University of Illinois.

(1) Yajima, S.; Hayashi, J.; Omori, M. *Chem. Lett.* **1975**, 931.
(2) Baney, R.; Chandra, G. In *Encyclopedia of Polymer Science and Engineering*; John Wiley and Sons: New York, 1988; Vol. 13, pp 312–44.
(3) Burns, G. T.; Saha, C. K.; Zank, G. A.; Freeman, H. A. *J. Mater. Sci.* **1992**, *27*, 2131–40.
(4) Atwell, W. H.; Burns, G. T.; Zank, G. A. In *Inorganic and Organometallic Polymers and Oligomers*; Kluwer Academic Publishers: Dordrecht, The Netherlands, **1990**; pp 147–59.
(5) Taylor, R. B.; Zank, G. A. *Polym. Prepr. (Am. Chem. Soc., Div. Poly Chem.)* **1991**, *32*, 586–7.
(6) (a) Alliegro, R. A.; Tinklepaugh, T. R. *J. Am. Ceram. Soc.* **1953**, *9*, A161. (b) Alliegro, R. A.; Coffin, L. B.; Tinklepaugh, T. R. *J. Am. Ceram. Soc.* **1956**, *12*, 386–9.
(7) Kamiya, K.; Makoto, O.; Yoko, T. *J. Non-Cryst. Solids* **1986**, *83*, 208.

0897-4756/92/2804-1313$03.00/0